From First-Principles to Quantum Electrodynamics: Part II – Benchmark Calculations for Isotopologues of the Hydrogen Molecule

Krzysztof Pachucki*,† and Jacek Komasa*,‡

†Faculty of Physics, University of Warsaw, Pasteura 5, 02-093 Warsaw, Poland
‡Faculty of Chemistry, Adam Mickiewicz University, Uniwersytetu Poznańskiego 8, 61-614 Poznań, Poland

E-mail: krp@fuw.edu.pl; komasa@man.poznan.pl

Abstract

Modern high-resolution spectroscopy of molecular hydrogen and its isotopologues has reached a level of accuracy at which subtle nonadiabatic, relativistic, and quantum electrodynamic (QED) effects can be probed and stringently tested. In our previous work (Part I), we introduced a fully nonadiabatic treatment of H_2 based on four-particle, explicitly correlated exponential basis functions, achieving relative accuracies of 10^{-9} for dissociation energies and rovibrational level spacings in the electronic ground state, in agreement with the most precise experimental data. In the present contribution (Part II), this methodology is applied to the remaining bound isotopologues of molecular hydrogen, including HD, HT, D_2, DT, and T_2, providing a unified high-precision theoretical description of their rovibrational structure. Within the same four-body framework, we evaluate the leading relativistic and QED corrections of the lowest rovibrational levels of the ground electronic state. For all isotopologues considered, dissociation energies and selected rovibrational transition frequencies are obtained with sub-MHz ($\sim 10^{-5}\,\mathrm{cm}^{-1}$) uncertainties. The resulting theoretical data are compared with the most precise spectroscopic measurements for each isotopologue and are found to be consistent within the combined uncertainties. The present calculations for the molecular hydrogen family achieve uncertainties previously attainable only for two- and three-body systems, such as hydrogen and helium atoms and the molecular ion H_2^+. Taken together, Parts I and II establish a coherent high-precision benchmark for the rovibrational spectra of molecular hydrogen isotopologues, including those containing tritium, and provide a stringent test of molecular quantum electrodynamics at the four-body level.

1 Introduction

One hundred years ago, on March 13, 1926, Erwin Schrödinger published his seminal paper introducing the wave equation that now bears his name.[1] Despite a century of intensive research, exact solutions of the Schrödinger equation remain available only for hydrogenic atoms, while molecular systems and non-hydrogenic atoms generally require approximate treatments. Nevertheless, for two- and three-body systems, such as the helium atom[2,3] or the molecular hydrogen cation,[4] solutions can be obtained with a precision far exceeding typical practical requirements. In recent years, nonrelativistic energies with 13–14 significant digits have also been achieved for four-body systems, such as the hydrogen molecule.[5]

Since the dawn of quantum mechanics, molecular hydrogen and its isotopologues have occupied a unique position in molecular physics and precision metrology. Owing to their exceptional simplicity and the rapid progress in high-resolution spectroscopy, these systems provide an ideal testing ground for quantum mechanics, relativistic effects, and quantum electrodynamics (QED) in a genuinely molecular context. Rovibrational transition frequencies of hydrogen isotopologues are now measured with sub-MHz accuracy ($1\,\mathrm{MHz} \approx 3.3 \times 10^{-5}\,\mathrm{cm}^{-1}$), and relative uncertainties can reach the 10^{-11} level.[6–10] Such experimental precision renders even subtle higher-order QED contributions observable. At the same time, the light nuclear masses lead to pronounced nonadiabatic effects, making a theoretical treatment beyond the Born–Oppenheimer approximation indispensable for an accurate description of the spectra.

The aforementioned precision in solving the Schrödinger equation for H_2 has been achieved using wave functions expanded in a basis of explicitly correlated exponential four-particle functions, referred to as nonadiabatic James–Coolidge (naJC) functions. In conjunction with this basis, a novel integration technique[11] for the efficient evaluation of matrix elements was developed. In the present work, we employ the same class of wave functions and a closely related integration strategy to evaluate the matrix elements entering the leading relativistic and QED corrections for the family of hydrogen-molecule isotopologues.

In Part I of this work,[12] the focus was on the parent isotopologue H_2. A fully nonadiabatic four-particle approach based on naJC basis functions enabled the calculation of essentially basis-set-limited nonrelativistic energies and the evaluation of relativistic and QED corrections using the same high-quality wave function. For H_2, this methodology produced dissociation energies and rovibrational level spacings in the electronic ground state with relative accuracies down to the 10^{-9} level, in excellent agreement with the most precise experimental data available and resolving previous discrepancies between theory and experiment.

The present article (Part II) extends the methodology introduced in Part I to the remaining isotopologues of molecular hydrogen: HD, HT, D_2, DT, and T_2. Applying the same theoretical framework, we evaluate the leading relativistic and QED corrections and determine dissociation energies and selected rovibrational transition frequencies with sub-megahertz uncertainties. This extension provides a consistent, high-precision theoretical description of the rovibrational structures across the entire molecular hydrogen family.

The paper is organized as follows. In section 2, we briefly summarize the theoretical framework introduced in Part I and discuss its extension to systems with unequal nuclear masses. Computational aspects are described, and numerical results are reported and analyzed in section 3, with a detailed comparison to available experimental data. Finally, section 4 provides a conclusion and outlook, including perspectives on further improvements.

To keep the article concise, we will not repeat the lengthy formulas from Part I; instead, we will provide references to the relevant equations. Moreover, to maintain a proper balance between text, tables, and figures, a large portion of the final and intermediate numerical data was placed in Supplementary Information files, one for each molecule.

2 Theoretical Framework

In this section, we briefly summarize the theoretical framework introduced in Part I and outline the modifications required to treat the remaining isotopologues of molecular hydrogen. The working equations, along with a detailed discussion of the numerical implementation, have been presented in Part I and will not be repeated here.

The theoretical framework underlying the present results is nonrelativistic quantum electrodynamics (NRQED).[13] Within this approach, the energy E of a bound rovibrational level of a light molecule is expressed as an expansion in powers of the fine-structure constant α,

$$E(\alpha) = m\,\alpha^2\,E^{(2)} + m\,\alpha^4\,E^{(4)} + m\,\alpha^5\,E^{(5)} + m\,\alpha^6\,E^{(6)} + m\,\alpha^7\,E^{(7)} + \dots\,, \tag{1}$$

where m denotes the electron mass. The expansion coefficients $E^{(n)}$ are determined as expectation values of effective NRQED operators evaluated with the nonrelativistic wave function Ψ.

2.1 Four-particle nonrelativistic Hamiltonian

All systems considered in this work are described at the nonrelativistic level by the four-particle Coulomb Hamiltonian for two electrons and two nuclei with charges q_a (in units of the elementary charge) and masses m_a (in units of the electron mass),

$$H^{(2)} = \frac{1}{2}\sum_{a=1}^{4}\frac{m}{m_a}\,p_a^2 + \sum_{a<b}\frac{q_a q_b}{r_{ab}}, \tag{2}$$

with the overall center-of-mass motion removed. The full four-particle Schrödinger equation $H^{(2)}\,\Psi = E^{(2)}\,\Psi$ is solved without invoking the Born–Oppenheimer, one-electron, or other common adiabatic approximations; all four particles are treated on an equal quantum-mechanical footing.

2.2 Explicitly correlated nonadiabatic wave function

The central ingredient of our approach is an explicitly correlated, nonadiabatic wave function expanded in the basis of exponential James-Coolidge-like functions of the interparticle distances. We write

$$\Psi = \sum_{\Lambda=0}^{2}\sum_{k=1}^{K} c_{\Lambda k}\,\psi_{\Lambda k}, \tag{3}$$

where the basis functions ψ_k depend explicitly on all six interparticle distances r_{ab} combined within elliptic-like coordinates: $\zeta_1 = r_{13} + r_{14}$, $\eta_1 = r_{13} - r_{14}$, $\zeta_2 = r_{23} + r_{24}$, $\eta_2 = r_{23} - r_{24}$, and $\vec{R} = \vec{r}_{34}$ and are parameterized by nonlinear exponents α_Λ and β_Λ optimized variationally:

$$\psi_{\Lambda k} = \mathcal{Q}_\Lambda\,e^{-\alpha_\Lambda R - \beta_\Lambda(\zeta_1+\zeta_2)}\,R^{k_0}\,r_{12}^{k_1}\,\eta_1^{k_2}\,\eta_2^{k_3}\,\zeta_1^{k_4}\,\zeta_2^{k_5} \tag{4}$$

The prefactor $\mathcal{Q}_\Lambda$ assigns a well-defined electronic angular momentum $\vec{L}$ to the basis function ψ_k, where Λ is the absolute value of the projection of $\vec{L}$ onto the internuclear axis (see Part I for more details). The remaining part of ψ_k ensures an accurate description of both short- and long-range correlation effects and provides a compact representation of the exact four-particle eigenstates.

For homonuclear isotopologues, the basis has the appropriate permutation symmetry with respect to interchange of the two nuclei and to reproduce the required gerade/ungerade spatial parity of the electronic motion. For heteronuclear isotopologues, the nuclear permutation symmetry is absent, and the corresponding symmetry constraints on the basis functions are relaxed; however, the treatment of electronic exchange and total angular momentum is identical to that used for H_2 in Part I. In all cases, the spin part of the wave function is chosen so as to yield an overall antisymmetric fermionic state.

The nonrelativistic energies are obtained by a standard Rayleigh–Ritz variational procedure applied to the four-particle Hamiltonian (2) in the naJC basis. The matrix elements of the Hamiltonian are evaluated analytically using the techniques reported in Refs. 5 and 14. The only source of nonrelativistic error in our calculations is the finite size of the exponential basis sets.

The non-linear parameters α_Λ and β_Λ are optimized to minimize the variational energy for individual rovibrational states. For each isotopologue, we construct large, state-specific basis sets and monitor the convergence of the energies with respect to both the size of the basis and the distribution of non-linear parameters. Residual basis-set incompleteness errors are estimated by comparing results from systematically enlarged basis sets. Table 1 presents a sample convergence of the nonrelativistic energy with increasing size K of the basis for the most demanding case of the heaviest heteronuclear isotopologue DT in a rotationally and vibrationally excited state. In conclusion, the absolute precision achieved for the nonrelativistic dissociation energy is $10^{-8}\,\mathrm{cm}^{-1}$ (10^{-13} relative) and its contribution to the overall error budget is negligible. The same concerns the remainig studied levels and isotopologues.[15–17]

Table 1: Convergence of the nonrelativistic energy $E^{(2)}$ and its contribution to dissociation energy $D^{(2)}$ for $v = 2, J = 4$ level of DT. $\Omega = \max\left(\sum_{i=1}^{5} k_i\right)$ is the electronic shell parameter.

Ω	$E^{(2)}$[a.u.]	$D^{(2)}$[cm^{-1}]
9	−1.141 156 984 864 03	31 030.226 097 836
10	−1.141 156 984 911 29	31 030.226 108 209
11	−1.141 156 984 919 69	31 030.226 110 054
12	−1.141 156 984 921 51	31 030.226 110 453
13	−1.141 156 984 922 05	31 030.226 110 571
14	−1.141 156 984 922 18	31 030.226 110 600
∞	−1.141 156 984 922 24(5)	31 030.226 110 61(1)

2.3 Relativistic corrections

Relativistic and QED effects are represented by subsequent terms of the α expansion (1). The leading relativistic contribution $E^{(4)}$ is described by the spin-independent Breit-Pauli Hamiltonian $H^{(4)}$, including the mass-velocity, Darwin, and orbit–orbit terms appropriate for the electronic singlet ground state; see Eq. (11) in Part I for detailed expressions. This correction is evaluated as an expectation value of $H^{(4)}$ with the naJC wave functions of Eqs. (3)-(4). Detailed convergence for individual components of $H^{(4)}$ in subsequent rovibrational levels is shown in Tables S1 of Supporting Information files relevant for each molecule. Below we present a small excerpt from this extensive data to illustrate the convergence of the relativistic correction.

Table 2: Convergence of the relativistic correction $E^{(4)}$ and its contribution to dissociation energy $D^{(4)}$ for $v = 2, J = 4$ level of DT. K is the basis set size and $\Omega = \max\left(\sum_{i=1}^{5} k_i\right)$ is the electronic shell parameter limiting this size.

Ω	K	$E^{(4)}$[a.u.]	$D^{(4)}$[cm^{-1}]
9	139832	−0.201 426 615 7	−0.567 692 873
10	209209	−0.201 426 328 5	−0.567 696 230
11	303520	−0.201 426 247 3	−0.567 697 179
12	429268	−0.201 426 210 7	−0.567 697 607
∞	∞	−0.201 426 18(3)	−0.567 698 0(4)

The convergence analysis can be summarized by noticing that an absolute uncertainty of the relativistic correction to dissociation energy is less than $4 \times 10^{-7}\,\mathrm{cm}^{-1}$ for rotational levels ($J > 0$) and less than $7 \times 10^{-8}\,\mathrm{cm}^{-1}$ for $J = 0$. This corresponds to relative errors of 7×10^{-7} and 1×10^{-7}, respectively. Such precision allows the uncertainty from $E^{(4)}$ to be neglected in the overall error budget.

Another relativistic contribution, often neglected due to its smallness, is the correction due to the finite size of the nucleus, $E^{(4)}_{\mathrm{fs}}$. The leading term of this correction is proportional to the expectation value of the electron-nucleus Dirac delta and depends also on a nuclear parameter called the root-mean-square charge radius of the nucleus, r_C^2, describing the spatial distribution of nuclear charge; see Eq. (12) in Part I. Since the Dirac-delta expectation value can be calculated using the naJC function to a very high precision, the factor limiting the precision of $E^{(4)}_{\mathrm{fs}}$ is the uncertainty in the experimental determination of r_C^2. The numerical values of this parameter used in this work for all three atomic nuclei are presented in Table 3, while the contributions to the dissociation energy of individual levels are listed in Tables S2 of Supporting Information.

Table 3: Root-mean-square charge radius of the nucleus, r_C^2, applied in this work.

Nucleus	r_C^2[fm^2]	Reference
Proton	0.84075(64)	18
Deuteron	2.12778(27)	18
Triton	1.7591(363)	19

An analysis of the contents of these tables shows that the largest contribution to the dissociation energy from $E^{(4)}_{\mathrm{fs}}$ is found in D_2, approximately $-2 \times 10^{-4}\,\mathrm{cm}^{-1}$ (≈ -6 MHz), and the smallest for HT, approximately $-7 \times 10^{-5}\,\mathrm{cm}^{-1}$ (≈ -2 MHz). This follows directly from the trend of the r_C^2 values given in Table 3. These values show that with the current precision of the calculations, the $E^{(4)}_{\mathrm{fs}}$ correction must be taken into account. As for the contribution to the error budget, only the uncertainties for tritium isotopologues are significant ($2 - 4 \times 10^{-6}\,\mathrm{cm}^{-1}$). This results from the relatively large r_C^2 error for triton.

2.4 QED corrections

The dominant $E^{(5)}$ QED effects are incorporated by means of effective one- and two-electron operators that account for the leading self-energy and vacuum-polarization corrections. The effective Hamiltonian is composed of five terms: electron-electron Dirac delta, electron-nucleus Dirac delta, analogous two Araki-Sucher terms, and the Bethe logarithm. The explicit forms of these operators have been presented in Eq. (13) of Part I. In the present work, we apply the same set of QED operators to all isotopologues. As before, the dominant Dirac-delta contributions were treated with the nonadiabatic James-Coolidge wave functions, while the Bethe logarithm and the Araki-Sucher terms were evaluated within the Born-Oppenheimer approximation using explicitly correlated Gaussian functions. Numerical results of the electron-nucleus Araki-Sucher component were published in Ref. 20, while those of the Bethe logarithm and the electron-electron Araki-Sucher terms in Ref. 21.

A novelty compared to the calculations for H_2 in Part I is the additional inclusion of nonadiabatic effects in the expectation value of the electron-electron Araki-Sucher operator. The method of evaluation of this correction was described in Ref. 22 and will be shortly outlined in this paragraph. The nonrelativistic Hamiltonian (2) can be split into the electronic and nuclear parts, $H^{(2)} = H_{\mathrm{el}} + H_{\mathrm{n}}$ ($m = 1$),

$$H_{\mathrm{el}} = -\frac{1}{2}\sum_a \nabla_a^2 + V \tag{5}$$

$$H_{\mathrm{n}} = -\frac{\nabla_R^2}{2\,\mu_{\mathrm{n}}} - \frac{\left(\sum_a \vec{\nabla}_a\right)^2}{2\,\mu_{\mathrm{n}}} - \left(\frac{1}{m_B} - \frac{1}{m_A}\right)\vec{\nabla}_R \cdot \sum_a \vec{\nabla}_a\,, \tag{6}$$

where V is the Coulomb potential operator and μ_{n} is the reduced mass of the nuclei A and B. The electron-electron Araki-Sucher operator $H^{(5)}_{\mathrm{AS,ee}} = -\frac{7\,\alpha^3}{6\,\pi}\frac{1}{r_{12}^3}$ can be treated as a perturbation to the electronic Hamiltonian with an auxiliary parameter ξ: $H^{\xi}_{\mathrm{el}} = H_{\mathrm{el}} + \xi\,H^{(5)}_{\mathrm{AS,ee}}$. Solution of the electronic Schrödinger equation $H^\xi_{\rm el}\varphi^\xi_{\rm el} = \mathcal{E}^\xi_{\rm el}\,\varphi^\xi_{\rm el}$ gives a ξ-dependent electronic wave function $\varphi^\xi_{\rm el}$. The expectation value of the nuclear Hamiltonian $H_{\rm n}$ evaluated with this wave function yields ξ-dependent adiabatic correction $\mathcal{E}^\xi_{\rm a}(R) = \left\langle \varphi^\xi_{\rm el}\,|H_{\rm n}|\,\varphi^\xi_{\rm el}\right\rangle$. Finally, the approximate nonadiabatic correction to the electron-electron Araki-Sucher term is evaluated as a numerical derivative of $\mathcal{E}^\xi_{\rm a}$

$$\mathcal{E}^{(5,1)}_{\rm AS,ee}(R) = \lim_{\xi\to 0}\left(\mathcal{E}^\xi_{\rm a} - \mathcal{E}^{-\xi}_{\rm a}\right)/(2\,\xi)\,. \tag{7}$$

The numerical contribution to the dissociation energy from this correction is small but non-negligible in the context of our target sub-MHz accuracy. Its value depends only weakly on the vibrational and rotational quantum numbers. It shifts the energy levels downward by $0.35\times10^{-5}\,\mathrm{cm}^{-1}$ (0.10 MHz) for the heaviest isotopologue T_2 and by $1.1\times10^{-5}\,\mathrm{cm}^{-1}$ (0.32 MHz) for the lightest H_2. Tables S3 in the Supporting Information provide the final values of the components constituting the leading QED correction to the dissociation energy.

2.5 Higher-order QED corrections

The $m\,\alpha^6$ correction is represented by a rather extensive effective Hamiltonian, so as in Part I, we refer the reader to the original paper Ref. 23 for all the details. The calculations of this correction were performed in the BO approximation using our publicly available program H2Spectre.[24] The estimated error has two sources: numerical and the neglected finite nuclear mass effects.[25] The contribution of $E^{(6)}$ to the dissociation energy ranges from $-1.6\times10^{-3}\,\mathrm{cm}^{-1}$ to $-2.1\times10^{-3}\,\mathrm{cm}^{-1}$ and varies apparently with the change of the vibrational state, depending weakly on the rotational state and on the isotopologue itself.

The full form of the expression $m\,\alpha^7$ is currently known only in the theory of hydrogen-like atoms. Drawing on experience from this theory, we estimated $E^{(7)}$ using a dominant term that accounts for the leading one- and two-loop radiative corrections; see Eq. (20) in Part I. We assess that the error due to unknown components is less than 25% of the total correction.

3 Results and Discussion

The primary outcome of our calculations is the dissociation energy of individual rovibrational levels, $D_{v,J}$ of the five isotpologues of the hydrogen molecule: HD, HT, D_2, DT, and T_2. Analogously to the total binding energy E (see Eq. (1)), $D_{v,J}$ is represented as a power series in α,

$$D_{v,J} = \sum_n D^{(n)}_{v,J}\,. \tag{8}$$

For each power of α we evaluate separately the contribution to the dissociation energy,

$$D^{(n)}_{v,J}(AB) = E^{(n)}(A) + E^{(n)}(B) - E^{(n)}(AB), \tag{9}$$

and express the result in units of cm^{-1}. The expressions for the hyperfine-averaged atomic energies have been presented in detail in Part I [see Eqs. (21)-(27)]; they are formulated consistently with the level of theory adopted for the molecular energies. We assume that uncertainties associated with the atomic $E^{(n)}$ contributions are negligible.

The resulting dissociation energies are collected in Table 4, while the individual $D^{(n)}_{v,J}$ components for each isotopologue are provided in Tables S2 of the Supporting Information. As already mentioned, the Supporting Information also includes tables illustrating the convergence of the relativistic expectation values for all studied levels. These results corroborate the achieved numerical precision, and the extrapolated infinite-basis values may serve as reference data for alternative approaches.

To ensure numerical stability, we employ quad-double precision arithmetic (64 digits) in all linear-algebra operations. The evaluation of individual matrix elements requires much higher precision, up to 370 digits. The matrices involved are large and dense, with the largest exceeding a dimension of 500 000. The combination of large matrix sizes and extended precision leads to extreme memory requirements—often several terabytes per matrix. As a result, parallelization becomes necessary not only for reducing wall-clock time but also for distributing memory usage. The computational cost for a single energy level amounts to several million core-hours, which limits the feasibility of treating all several thousand rovibrational levels of the six hydrogen isotopologues. Consequently, we restrict the study to a selected set of low-lying states, including those relevant to the most precise spectroscopic measurements.

In the following subsections we will discuss the results obtained for individual isotopologues. The starting point is the dissociation energy of successive rovibrational levels. Differences between these energies yield transition frequencies, expressed in megahertz. While the estimated uncertainty of dissociation energies is typically well described by the convergence of operator expectation values or by the magnitude of neglected physical effects, transition frequencies involve subtracting two quantities that each carry uncertainties. This introduces the issue of potential error cancellation, which is difficult to quantify. To address this, we adopt a simple yet conservative procedure: for each transition, we assign the larger of the uncertainties associated with the two levels involved. This approach intentionally overestimates the error to ensure we remain on the safe side.

Particular emphasis is placed on comparison of our theoretical predictions with available spectroscopic data. In many cases, experimental results clearly surpass the accuracy of the theoretical values and therefore serve as the ultimate benchmark for the present methodology. In other cases, where the theory is more accurate than the measurements, the results provide motivation for refined experimental studies. The most exciting perspective concerns transitions that have not yet been measured but fall within the range accessible to high-precision spectroscopy, enabling future validation of our predictions.

3.1 HD

Alongside H_2, the HD molecule remains the most extensively studied isotopologue in high-resolution molecular spectroscopy. The experimental dissociation energies, $36\,405.783\,66(36)\,\mathrm{cm}^{-1}$ reported by Sprecher et al.[26] and $36\,405.782\,53(7)\,\mathrm{cm}^{-1}$ from the more recent measurement of Hussels et al.,[27] continue to serve as primary benchmarks

Table 4: Theoretically predicted dissociation energy $D_{v,J}$ for several lowest rotational levels in the vibrational states v of hydrogen isotopologues [cm^{-1}]. Components of $D_{v,J}$ related to subsequent terms $E^{(n)}$ of the α-expansion (1) are shown in Supporting Information.

(v,J)	$D_{v,J}$	(v,J)	$D_{v,J}$	(v,J)	$D_{v,J}$
			HD		
(0,0)	36 405.782 473(26)	(1,0)	32 773.622 044(25)	(2,0)	29 318.905 449(25)
(0,1)	36 316.554 543(26)	(1,1)	32 688.250 141(25)	(2,1)	29 237.312 099(25)
(0,2)	36 138.713 277(26)	(1,2)	32 518.103 116(25)	(2,2)	29 074.705 182(25)
(0,3)	35 873.473 188(26)	(1,3)	32 264.360 068(25)	(2,3)	28 832.230 046(26)
(0,4)	35 522.620 180(25)	(1,4)	31 928.754 333(25)	(2,4)	28 511.570 007(26)
			HT		
(0,0)	36 512.199 563(26)	(1,0)	33 077.386 277(25)	(2,0)	29 800.664 721(25)
(0,1)	36 432.746 870(26)	(1,1)	33 001.171 385(25)	(2,1)	29 727.625 059(25)
(0,2)	36 274.328 185(26)	(1,2)	32 849.214 980(25)	(2,2)	29 582.006 365(25)
(0,3)	36 037.906 560(26)	(1,3)	32 622.453 614(25)	(2,3)	29 364.719 849(25)
(0,4)	35 724.901 234(26)	(1,4)	32 322.267 134(25)	(2,4)	29 077.107 747(25)
			D_2		
(0,0)	36 748.362 339(26)	(1,0)	33 754.745 274(25)	(2,0)	30 880.241 921(24)
(0,1)	36 688.581 725(26)	(1,1)	33 697.074 717(25)	(2,1)	30 824.644 594(24)
(0,2)	36 569.295 240(26)	(1,2)	33 582.001 813(25)	(2,2)	30 713.711 857(24)
(0,3)	36 391.047 984(26)	(1,3)	33 410.058 644(25)	(2,3)	30 547.963 260(24)
(0,4)	36 154.646 794(26)	(1,4)	33 182.032 658(24)	(2,4)	30 328.167 590(24)
(2,5)	30 055.330 698(23)	(2,6)	29 730.679 991(24)	(3,0)	28 122.760 404(23)
			DT		
(0,0)	36 881.281 200(27)	(1,0)	34 137.939 455(25)	(2,0)	31 494.181 205(24)
(0,1)	36 831.345 876(27)	(1,1)	34 089.613 787(25)	(2,1)	31 447.438 946(24)
(0,2)	36 731.666 624(26)	(1,2)	33 993.149 651(25)	(2,2)	31 354.137 606(24)
(0,3)	36 582.623 652(26)	(1,3)	33 848.918 987(25)	(2,3)	31 214.641 111(24)
(0,4)	36 384.780 986(26)	(1,4)	33 657.473 442(25)	(2,4)	31 029.489 118(24)
			T_2		
(0,0)	37 028.496 244(27)	(1,0)	34 563.992 088(25)	(2,0)	32 179.466 707(24)
(0,1)	36 988.433 236(27)	(1,1)	34 525.084 883(25)	(2,1)	32 141.698 030(24)
(0,2)	36 908.430 194(27)	(1,2)	34 447.391 018(25)	(2,2)	32 066.278 891(24)
(0,3)	36 788.731 717(27)	(1,3)	34 331.150 338(25)	(2,3)	31 953.444 496(24)
(0,4)	36 629.701 469(26)	(1,4)	34 176.719 353(25)	(2,4)	31 803.544 420(24)
(0,5)	36 431.818 357(26)	(1,5)	33 984.567 508(25)	(2,5)	31 617.038 923(24)

for evaluating theoretical descriptions of the system. Our present theoretical determination of $D_{0,0}$ (see Table 4) reproduces the earlier explicitly correlated Gaussian result, $36\,405.782\,477(26)\,\mathrm{cm}^{-1}$,[28] and remains fully consistent with both experimental values, yielding a residual deviation of only $0.000\,06(7)\,\mathrm{cm}^{-1}$.

HD spectroscopy exploits its small, permanent dipole moment, which results in dipole-allowed rovibrational transitions of much higher intensity than in H_2 or D_2. Techniques such as Doppler-broadened cavity ring-down absorption spectroscopy at room temperature[29] or in cryogenic conditions,[30] molecular-beam double-resonance spectroscopy,[31] and NICE-OHMS,[32] combined with optical-frequency-comb calibration, now achieve kHz-level accuracy for both fundamental and overtone bands. Experimental data for these bands and pure rotational transitions provide stringent benchmarks for *ab initio* calculations that include relativistic and QED contributions. While previous comparisons revealed persistent MHz-level discrepancies in certain bands, these inconsistencies are no longer present in our results due to the explicit inclusion of finite-nuclear-mass effects in the relativistic and QED corrections.

Currently, the HD literature includes 13 rovibrational transitions measured with uncertainties below 1 MHz. Using the energy levels from Table 4, we calculated the corresponding theoretical transition frequencies and compiled them in Table 5 alongside the experimental values. The final column lists the differences between theory and experiment, along with the combined uncertainties. For all transitions considered, agreement is achieved within the stated uncertainties. It is worth noting, however, that some experimental data are an order of magnitude more accurate than the theoretical predictions and these uncertainties are largely determined by the error of the theory. Figure 1 provides a graphical comparison that offers a clear visual assessment of the overall consistency between experiment and theory.

Table 5: Comparison of theoretically predicted transition frequencies (in MHz) for HD with 13 experimental results that were measured with sub-MHz accuracy. CODATA 2022 recommended physical constants were used.[18]

Line	ν_{the}	ν_{exp}	$\Delta\nu$
0-0 R(0)	2 674 986.06(78)	2 674 986.094(25)[a]	−0.04(78)
0-0 S(0)	8 006 533.07(78)	8 006 533.168(26)[b]	−0.10(78)
0-0 S(1)	13 283 244.85(79)	13 283 245.098(30)[c]	−0.25(79)
2-2 S(1)	12 144 054.42(78)	12 144 054.660(20)[b]	−0.24(78)
2-2 S(2)	16 882 367.82(79)	16 882 368.179(20)[c]	−0.36(79)
1-0 R(0)	111 448 815.54(81)	111 448 815.477(13)[d]	0.06(81)
2-0 P(1)	209 784 242.20(88)	209 784 242.007(20)[e]	0.19(88)
2-0 R(0)	214 905 335.36(88)	214 905 335.185(20)[f]	0.17(88)
2-0 P(2)	206 898 802.29(87)	206 898 802.15(15)[b]	0.14(88)
2-0 R(1)	217 105 182.01(88)	217 105 181.898(20)[f]	0.12(88)
2-0 P(3)	203 821 937.16(87)	203 821 936.805(60)[c]	0.36(87)
2-0 R(2)	219 042 856.71(89)	219 042 856.621(28)[g]	0.09(89)
2-0 R(3)	220 704 304.99(89)	220 704 304.951(28)[g]	0.03(89)

[a]Druin et al., 2011;[33] [b]Cozijn et al., 2022;[34] [c]Cozijn et al., 2022;[35] [d]Fast and Meek, 2020;[31] [e]Diouf et al., 2020;[36] [f]Kassi et al., 2022;[30] [g]Cozijn et al., 2018;[32]

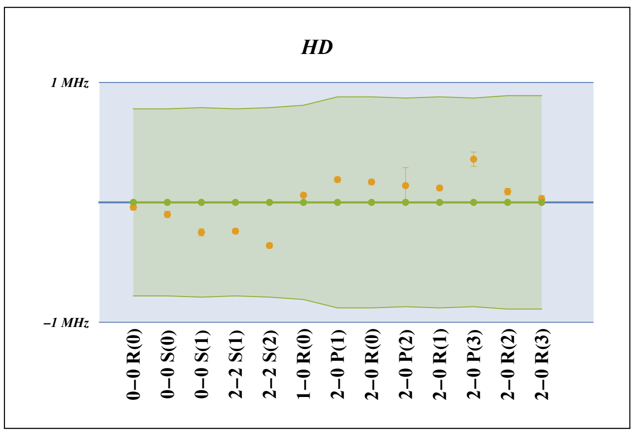

Figure 1: Differences between theoretically predicted and experimental line positions for HD shown against the ±1 MHz error band (in blue) and the theoretical error band (in green). The error bars around the dots come from the experiment.

3.2 D_2

High-precision spectroscopy of the D_2 molecule is another source of a rigorous benchmark for contemporary *ab initio* methodologies. The absence of a permanent dipole moment in homonuclear molecules means that rovibrational transitions are predominantly governed by weak electric-quadrupole interactions, inherently restricting experimental precision. Recent advancements have substantially mitigated these limitations. Notably, the application of strong static electric fields has induced a transient dipole moment in D_2, thereby amplifying otherwise forbidden transition strengths and enabling high-resolution spectroscopy in supersonic molecular beams. Employing this field-induced dipole approach, the $S_1(0)$ transition was measured with an absolute uncertainty of 17 kHz,[37] representing nearly an order-of-magnitude improvement over previous results. The previously mentioned cavity ring-down spectroscopy can also provide accurate results when coupled with a frequency comb referenced to a primary frequency standard.[38,39]

Table 6: Comparison of theoretically predicted transition frequencies (in MHz) for D_2 with seven experimental results that were measured with sub-MHz accuracy. CODATA 2022 recommended physical constants were used.[18]

Line	ν_{the}	ν_{exp}	$\Delta\nu$
1-0 S(0)	94 925 100.50(80)	94 925 100.487(17)[a]	0.02(80)
2-0 Q(1)	175 796 412.58(82)	175 796 410.24(87)[b]	2.3(12)
2-0 Q(2)	175 545 973.55(81)	175 545 972.79(42)[b]	0.76(92)
2-0 S(0)	180 914 270.12(82)	180 914 269.55(30)[b]	0.57(88)
2-0 S(2)	187 104 299.90(82)	187 104 300.40(17)[c]	−0.50(84)
2-0 S(3)	189 940 025.84(83)	189 940 027.01(87)[d]	−1.2(12)
2-0 S(4)	192 585 679.80(83)	192 585 682.11(99)[d]	−2.3(13)

[a]Fast and Meek, 2022;[37] [b]Mondelain et al., 2020;[39] [c]Zaborowski et al., 2020;[40] [d]Wójtewicz et al., 2020;[41]

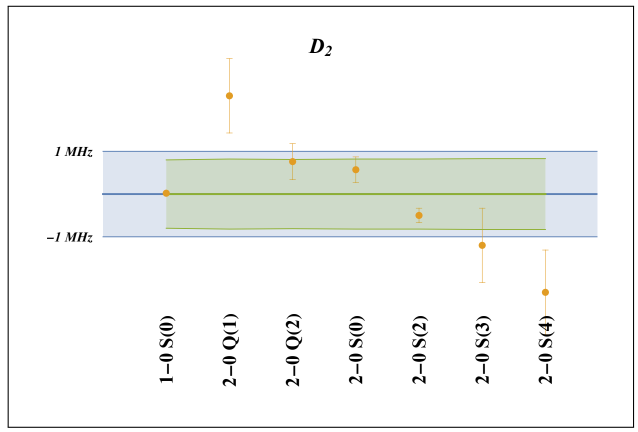

Figure 2: Differences between theoretically predicted and experimental line positions for D_2 shown against the ±1 MHz error band (in blue) and the theoretical error band (in green). The error bars around the dots come from the experiment.

In the context of the present computations, the experimental reference values relevant for assessing the accuracy of the theoretical treatment include the high-precision dissociation energy of 36 748.362 282(26) cm^{-1} reported by Hussels et al.,[27] as well as the earlier determination of Liu et al.,[42] 36 748.362 86(68) cm^{-1}, which remains consistent with both modern theory and experiment owing to its larger uncertainty. Previous high-precision calculations employing explicitly correlated Gaussian (ECG) basis functions yielded 36 748.362 342(26) cm^{-1},[28] and the deviation between this theoretical prediction and the most precise experimental result amounts to $6.0 \times 10^{-5}\,\text{cm}^{-1}$ (1.8 MHz), corresponding to approximately 2σ. The updated evaluation reported here (see Table 4) confirms the earlier theoretical value, and the slight 2σ deviation therefore persists.

Within the published measurements of rovibrational transition energies in D_2, seven transitions have been determined with sub-MHz precision. Table 6 summarizes these experimental values alongside our theoretical predictions. As illustrated in both the table and Figure 2, three of the measured frequencies deviate from our theoretical results by more than 1 MHz, though all remain within the 2σ combined uncertainty range. The underlying cause of these discrepancies is currently unknown; however, it is noteworthy that the relevant experiments exhibit relatively large error bars (0.87–0.99 MHz) and that the deviations do not show any systematic pattern.

3.3 HT, DT, T_2

High-precision studies of tritiated hydrogen isotopologues (HT, DT, and T_2) are partly motivated by the KATRIN program,[43] which determines the absolute neutrino mass from the T_2 β-decay endpoint and has set $m_\nu < 0.45$ eV. In its current phase, KATRIN also searches for sterile neutrinos through subtle distortions in the β-decay spectrum,[44] motivating improved theoretical descriptions and high-fidelity measurements for HT, DT, and T_2. However, high-precision spectroscopy of tritiated hydrogen isotopologues faces unique constraints due to the limited availability of tritium and strict radiation-safety regulations. Under these conditions, recent rovibrational measurements of these isotopologues[45–47] represent a significant experimental accomplishment.

Table 7: Comparison of theoretically predicted transition frequencies (in MHz) for HT, DT, and T_2 with the most accurate experimental data. CODATA 2022 recommended physical constants were used.[18]

	HT		
Line	ν_{the}	ν^a_{exp}	$\Delta\nu$
2-0 P(1)	198 824 820.93(85)	198 824 820.60(10)	0.33(86)
2-0 R(0)	203 396 426.70(85)	203 396 426.692(21)	0.00(85)
2-0 R(1)	205 380 033.52(85)	205 380 033.644(22)	−0.12(85)
	DT		
Line	ν_{the}	ν^b_{exp}	$\Delta\nu$
1-0 Q(0)	82 243 316.47(80)	82 243 312.(13)	4(13)
1-0 Q(1)	82 195 060.23(80)	82 195 059.(12)	1(12)
1-0 Q(2)	82 098 673.46(80)	82 098 663.(13)	10(13)
1-0 Q(3)	81 954 404.07(79)	81 954 408.(13)	−4(13)
1-0 Q(4)	81 762 623.23(78)	81 762 620.(13)	3(13)
	T_2		
Line	ν_{the}	ν^b_{exp}	$\Delta\nu$
1-0 Q(0)	73 883 975.85(80)	73 883 969.(20)	7(20)
1-0 Q(1)	73 849 325.78(80)	73 849 320.(13)	6(13)
1-0 Q(2)	73 780 098.37(80)	73 780 098.(13)	0(13)
1-0 Q(3)	73 676 436.23(80)	73 676 435.(13)	1(13)
1-0 Q(4)	73 538 553.82(79)	73 538 560.(13)	−6(13)
1-0 Q(5)	73 366 734.74(78)	73 366 728.(13)	7(13)

[a]Cozijn *et al.*, 2024;[48] [b]Lai et al., 2020;[49]

From the theoretical perspective, studies of T-containing molecules do not suffer from the complications associated with radioactive samples. Their computational complexity is comparable to that of the stable isotopologues, though the substantial triton mass yields a more compact nuclear wavefunction. Achieving high accuracy therefore requires basis functions with higher powers of the internuclear coordinate R, increasing both the basis-set dimension and the computational cost. Among the tritiated species, DT is the most demanding case, as it is the heaviest heteronuclear isotopologue. For example, the Hamiltonian matrix for the $(2,0)$ vibrational–rotational level of DT exceeds half a million elements in dimension, making diagonalization of the associated dense matrices a nontrivial numerical task.

To our knowledge, no experimental determinations of the dissociation energies of T-isotopologues have been reported. Theoretical predictions, summarized in Table 4, therefore remain the sole source of this information. Based on agreement with experimentally benchmarked results for H_2, HD, and D_2, it is reasonable to assume that the accuracy achieved for the T-containing species is of similar quality.

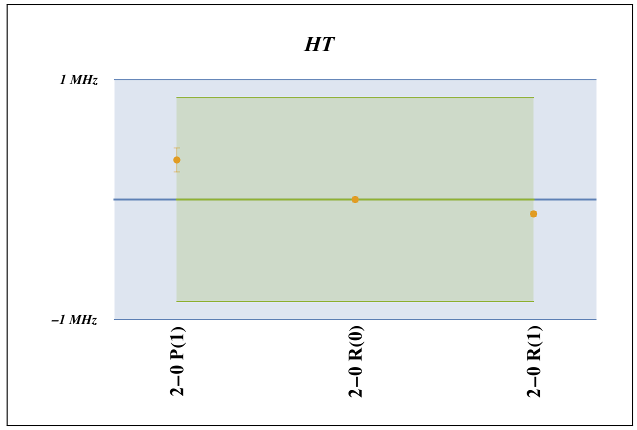

Figure 3: Differences between theoretically predicted and experimental line positions for HT shown against the ±1 MHz error band (in blue) and the theoretical error band (in green). The error bars around the dots come from the experiment.

In contrast, modern measurements of rovibrational transition frequencies in the fundamental and first-overtone bands of HT, DT, and T_2 are available. In general, the accuracy achieved for the rovibrational splittings in these isotopologues is on the order of 10 MHz.[46,47,49] Most recently, a sophisticated measurements on selected transitions in HT with 0.02 MHz precision were reported[48] challenging our theoretical predictions. A direct comparison between theory and the most accurate experimental data is presented in Table 7. This comparison reveals a full agreement within the assigned combined uncertainties. In particular, the theoretical line positions for HT fully reproduce the extremely precise measurements of Ref. 48. The residual differences between experiment and theory for all three isotopologues are illustrated in Figures 3, 4, and 5.

4 Conclusion

The inclusion of finite nuclear mass effects in the relativistic and QED corrections, which is the main achievement of this work, resolves the previously reported 1–3 MHz discrepancy between theoretical and experimental frequencies. Sub-MHz agreement between theory and experiment is demonstrated for more than 30 of the most accurately measured transition frequencies available for H_2, HD, HT, and D_2.

The fully *ab initio* method presented in this study, relying on a limited set of physical constants, achieved relative accuracies of 7.1×10^{-10} for dissociation energies of rovibrational levels and 4×10^{-9} for transition frequencies. By comparison, the most accurate spectroscopic measurements in HD attain a precision of 9.2×10^{-11} (see Refs. 30 and 32), that is,

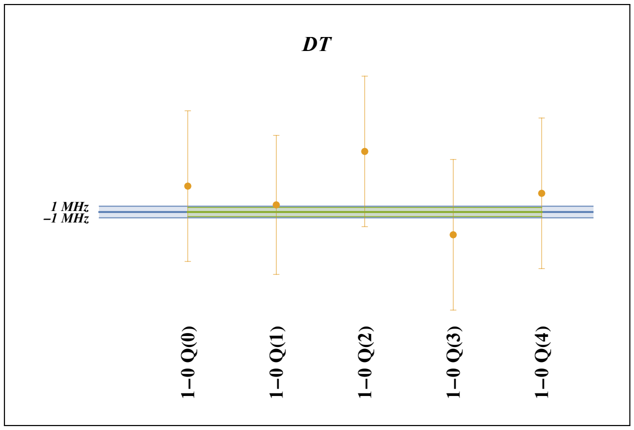

Figure 4: Differences between theoretically predicted and experimental line positions for DT shown against the ±1 MHz error band (in blue) and the theoretical error band (in green). The error bars around the dots come from the experiment.

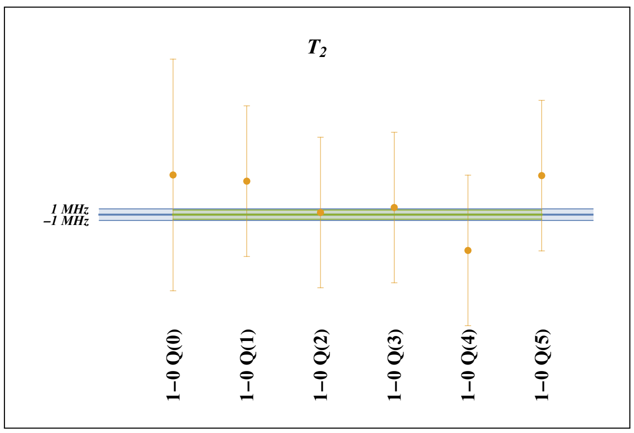

Figure 5: Differences between theoretically predicted and experimental line positions for T_2 shown against the ±1 MHz error band (in blue) and the theoretical error band (in green). The error bars around the dots come from the experiment.

approximately 40 times higher. At this level of experimental accuracy, high-resolution spectroscopy enables stringent, quantitative tests of relativistic and quantum electrodynamics (QED) effects, which contribute to molecular transition frequencies at the level of $\sim 10^3$ MHz and are now resolved with a relative accuracy of about 2×10^{-5}, thereby validating current calculations and exposing their current limits.

The dissociation energy is directly related to another measurable quantity—the molecular ionization energy E_I:

$$E_I(AB) = D_{0,0}(AB) + E_I(A) + E_I(B) - E_I(AB^+)\,. \quad (10)$$

Because the ionization energies of hydrogen and deuterium atoms and their molecular ions AB^+ have been calculated with two orders of magnitude greater precision, the uncertainty in $D_{0,0}(AB)$ can be effectively transferred to $E_I(AB)$. Using literature theoretical values for the ionization energies of H and D atoms[50,51] and corresponding molecular ions,[52] the $E_I(AB)$ can be evaluated to a high accuracy – the results are summarized in Table 8. These findings demonstrate a relative accuracy of 2.1×10^{-10}, underscoring the high precision now achievable for four-body molecular systems.

Table 8: Comparison of theoretically predicted ionization energy E_I (in cm^{-1}) for H_2, HD, and D_2 with the most accurate experimental results.

Mol.	Theory	Experiment	Difference
H_2	124 417.491 122(26)	124 417.491 13(37)^a	−0.000 01(37)
HD	124 568.484 604(26)	124 568.484 66(7)^b	−0.000 06(8)
D_2	124 745.393 796(26)	124 745.393 739(26)^c	0.000 057(37)

^{a}Liu et al., 2009;[53] ^{b}Hölsch et al., 2023;[54] ^{c}Hussels et al., 2022;[27]

Table 8 also presents a comparison of theoretical and experimental ionization energies. However, the reported experimental values depend on both direct measurements and theoretical determinations for atoms and molecular ions, so the compared values are not fully independent of each other.

To guide further improvements in accuracy, Figure 6 illustrates the distribution of the error budget among the individual contributions from the α expansion, using $D_{0,0}$ for HD as an example. The α^7 term contributes most significantly to the uncertainty. Since its complete form remains unknown, substantial theoretical work is required. Additional challenges include the fully nonadiabatic calculation of the α^6 correction, as well as of two components of the α^5 term: the Bethe logarithm and the Araki-Sucher corrections.

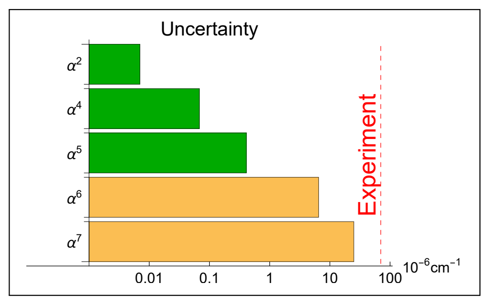

Figure 6: Error budget for the dissociation energy of HD. The uncertainties are shown on a logarithmic scale in units of 10^{-6} cm^{-1}. The green bars corresponding to α^2, α^4, and α^5 indicate the current precision achieved by accounting for finite nuclear mass effects. The α^6 and α^7 terms remain the dominant accuracy-limiting factors.

Acknowledgements

This research was supported by the National Science Center (Poland) Grant No. 2021/41/B/ST4/00089. A computer grant from the Poznań Supercomputing and Networking Center was used to carry out the numerical calculations.

Supporting Information Available

Supporting Information is available free of charge via the Internet at https://pubs.acs.org. The Supporting Information files: Supporting Information HD.pdf, Supporting Information HT.pdf, Supporting Information D2.pdf, Supporting Information DT.pdf, and Supporting Information T2.pdf contain numerical data for relativistic expectation values as well as the leading relativistic and quantum electrodynamic (QED) contributions to the dissociation energies of individual rovibrational levels.

References

(1) Schrödinger, E. Quantisierung als Eigenwertproblem. Erste Mitteilung. *Annalen der Physik* **1926**, *79*, 361–376.

(2) Korobov, V. I. Nonrelativistic Ionization Energy for the Helium Ground State. *Phys. Rev. A* **2002**, *66*, 024501.

(3) Schwartz, C. Further Computations of the He Atom Ground State. 2006; https://arxiv.org/abs/math-ph/0605018.

(4) Hijikata, Y.; Nakashima, H.; Nakatsuji, H. Solving non-Born–Oppenheimer Schrödinger equation for hydrogen molecular ion and its isotopomers using the free complement method. *J. Chem. Phys.* **2009**, *130*, 024102.

(5) Pachucki, K.; Komasa, J. Schrödinger equation solved for the hydrogen molecule with unprecedented accuracy. *J. Chem. Phys.* **2016**, *144*, 164306.

(6) Fleurbaey, H.; Koroleva, A. O.; Kassi, S.; Campargue, A. The high-accuracy spectroscopy of H_2 rovibrational transitions in the (2-0) band near 1.2 μm. *Phys. Chem. Chem. Phys.* **2023**, *25*, 14749–14756.

(7) Lamperti, M.; Rutkowski, L.; Ronchetti, D.; Gatti, D.; Gotti, R.; Cerullo, G.; Thibault, F.; Jóźwiak, H.; Wójtewicz, S.; Masłowski, P.; Wcisło, P.; Polli, D.; Marangoni1, M. Stimulated Raman scattering metrology of molecular hydrogen. *Commun. Phys.* **2023**, *6*, 67.

(8) Cozijn, F. M. J.; Diouf, M. L.; Ubachs, W. Lamb Dip of a Quadrupole Transition in H_2. *Phys. Rev. Lett.* **2023**, *131*, 073001.

(9) Diouf, M. L.; Cozijn, F. M. J.; Ubachs, W. Hyperfine structure in a vibrational quadrupole transition of ortho-H_2. *Mol. Phys.* **2024**, *122*, e2304101.

(10) Stankiewicz, K.; Makowski, M.; Słowiński, M.; Sołtys, K. L.; Bednarski, B.; Jóźwiak, H. J.; Stolarczyk, N.; Narożnik, M.; Kierski, D.; Wójtewicz, S.; Cygan, A.; Kowzan, G.; Masłowski, P.; Piwiński, M.; Lisak, D.; Wcisło, P. Cavity-Enhanced Spectroscopy in the Deep Cryogenic Regime for Quantum Sensing and Metrology. *Nat. Phys.* **2026**,

(11) Pachucki, K.; Komasa, J. Integrals for relativistic nonadiabatic energies of H_2 in an exponential basis. *Phys. Rev. A* **2024**, *109*, 032822.

(12) Pachucki, K.; Komasa, J. From First-Principles to Quantum Electrodynamics: Pushing the Limits of Theory with the Hydrogen Molecule. *J. Chem. Theory Comput.* **2025**, *21*, 12664–12673.

(13) Caswell, W. E.; Lepage, G. P. Effective lagrangians for bound state problems in QED, QCD, and other field theories. *Phys. Lett. B* **1986**, *167*, 437.

(14) Pachucki, K.; Komasa, J. Nonadiabatic rotational states of the hydrogen molecule. *Phys. Chem. Chem. Phys.* **2018**, *20*, 247–255.

(15) Pachucki, K.; Komasa, J. Nonrelativistic energy levels of HD. *Phys. Chem. Chem. Phys.* **2018**, *20*, 26297–26302.

(16) Pachucki, K.; Komasa, J. Nonrelativistic energy levels of D_2. *Phys. Chem. Chem. Phys.* **2019**, *21*, 10272–10276.

(17) Pachucki, K.; Komasa, J. Nonrelativistic energy of tritium-containing hydrogen molecule isotopologues. *Mol. Phys.* **2022**, *120*, e2040627.

(18) Mohr, P. J.; Newell, D. B.; Taylor, B. N.; Tiesinga, E. CODATA recommended values of the fundamental physical constants: 2022. *Rev. Mod. Phys.* **2025**, *97*, 025002.

(19) Angeli, I.; Marinova, K. P. Table of experimental nuclear ground state charge radii: An update. *Atomic Data and Nuclear Data Tables* **2013**, *99*, 69–95.

(20) Komasa, J. Electron-nucleus Araki-Sucher correction in the hydrogen molecule isotopologues. *Phys. Rev. A* **2026**, *113*, 012802.

(21) Siłkowski, M.; Pachucki, K.; Komasa, J.; Puchalski, M. Leading-order QED effects in the ground electronic state of molecular hydrogen. *Phys. Rev. A* **2023**, *107*, 032807.

(22) Pachucki, K.; Siłkowski, M. Nonadiabatic corrections to electric quadrupole transition rates in H_2. *Mol. Phys.* **2025**, e2603620.

(23) Puchalski, M.; Komasa, J.; Czachorowski, P.; Pachucki, K. Complete $\alpha^6 m$ Corrections to the Ground State of H_2. *Phys. Rev. Lett.* **2016**, *117*, 263002.

(24) H2Spectre ver. 7.4 Fortran source code 2022; https://www.fuw.edu.pl/~krp/;https://qcg.home.amu.edu.pl/H2Spectre.html.

(25) Komasa, J.; Puchalski, M.; Czachorowski, P.; Łach, G.; Pachucki, K. Rovibrational energy levels of the hydrogen molecule through nonadiabatic perturbation theory. *Phys. Rev. A* **2019**, *100*, 032519.

(26) Sprecher, D.; Liu, J.; Jungen, C.; Ubachs, W.; Merkt, F. Communication: The ionization and dissociation energies of HD. *J. Chem. Phys.* **2010**, *133*, 111102.

(27) Hussels, J.; Hölsch, N.; Cheng, C.-F.; Salumbides, E. J.; Bethlem, H. L.; Eikema, K. S. E.; Jungen, C.; Beyer, M.; Merkt, F.; Ubachs, W. Improved ionization and dissociation energies of the deuterium molecule. *Phys. Rev. A* **2022**, *105*, 022820.

(28) Puchalski, M.; Komasa, J.; Spyszkiewicz, A.; Pachucki, K. Dissociation energy of molecular hydrogen isotopologues. *Phys. Rev. A* **2019**, *100*, 020503.

(29) Castrillo, A.; Fasci, E.; Gianfrani, L. Doppler-limited precision spectroscopy of HD at 1.4 μm: An improved determination of the $R(1)$ center frequency. *Phys. Rev. A* **2021**, *103*, 022828.

(30) Kassi, S.; Lauzin, C.; Chaillot, J.; Campargue, A. The (2-0) $R(0)$ and $R(1)$ transition frequencies of HD determined to a 10^{-10} relative accuracy by Doppler spectroscopy at 80 K. *Phys. Chem. Chem. Phys.* **2022**, *24*, 23164–23172.

(31) Fast, A.; Meek, S. A. Sub-ppb Measurement of a Fundamental Band Rovibrational Transition in HD. *Phys. Rev. Lett.* **2020**, *125*, 023001.

(32) Cozijn, F. M. J.; Dupré, P.; Salumbides, E. J.; Eikema, K. S. E.; Ubachs, W. Sub-Doppler Frequency Metrology in HD for Tests of Fundamental Physics. *Phys. Rev. Lett.* **2018**, *120*, 153002.

(33) Drouin, B. J.; Yu, S.; Pearson, J. C.; Gupta, H. Terahertz spectroscopy for space applications: 2.5-2.7 THz spectra of HD, H_2O and NH_3. *J. Mol. Spectrosc.* **2011**, *1006*, 2 – 12.

(34) Cozijn, F. M. J.; Diouf, M. L.; Ubachs, W. Saturation spectroscopy of R(0), R(2) and P(2) lines in the (2-0) band of HD. *Eur. Phys. J. D* **2022**, *76*, 220.

(35) Cozijn, F. M. J.; Diouf, M. L.; Hermann, V.; Salumbides, E. J.; Schlösser, M.; Ubachs, W. Rotational level spacings in HD from vibrational saturation spectroscopy. *Phys. Rev. A* **2022**, *105*, 062823.

(36) Diouf, M. L.; Cozijn, F. M. J.; Lai, K.-F.; Salumbides, E. J.; Ubachs, W. Lamb-peak spectrum of the HD (2-0) $P(1)$ line. *Phys. Rev. Research* **2020**, *2*, 023209.

(37) Fast, A.; Meek, S. A. Precise measurement of the D_2 $S_1(0)$ vibrational transition frequency. *Mol. Phys.* **2022**, *120*, e1999520.

(38) Wcisło, P.; Thibault, F.; Zaborowski, M.; Wójtewicz, S.; Cygan, A.; Kowzan, G.; Masłowski, P.; Komasa, J.; Puchalski, M.; Pachucki, K.; Ciuryło, R.; Lisak, D. Accurate deuterium spectroscopy for fundamental studies. *J. Quant. Spectrosc. Radiat. Transfer* **2018**, *213*, 41 – 51.

(39) Mondelain, D.; Kassi, S.; Campargue, A. Transition frequencies in the (2-0) band of D_2 with MHz accuracy. *J. Quant. Spectrosc. Radiat. Transfer* **2020**, *253*, 107020.

(40) Zaborowski, M.; Słowiński, M.; Stankiewicz, K.; Thibault, F.; Cygan, A.; Jóźwiak, H.; Kowzan, G.; Masłowski, P.; Nishiyama, A.; Stolarczyk, N.; Wójtewicz, S.; Ciuryło, R.; Lisak, D.; Wcisło, P. Ultrahigh finesse cavity-enhanced spectroscopy for accurate tests of quantum electrodynamics for molecules. *Opt. Lett.* **2020**, *45*, 1603–1606.

(41) Wójtewicz, S.; Gotti, R.; Gatti, D.; Lamperti, M.; Laporta, P.; Jóźwiak, H.; Thibault, F.; Wcisło, P.; Marangoni, M. Accurate deuterium spectroscopy and comparison with ab initio calculations. *Phys. Rev. A* **2020**, *101*, 052504.

(42) Liu, J.; Sprecher, D.; Jungen, C.; Ubachs, W.; Merkt, F. Determination of the ionization and dissociation energies of the deuterium molecule D_2. *J. Chem. Phys.* **2010**, *132*, 154301.

(43) KATRIN Collaboration KATRIN – Karlsruhe Tritium Neutrino Experiment. https://www.katrin.kit.edu, Accessed: 2026-03-19.

(44) Collaboration, T. K. Sterile-neutrino search based on 259 days of KATRIN data. *Nature* **2025**, *648*, 70–75, Published online: 3 December 2025.

(45) Schlösser, M.; Zhao, X.; Trivikram, M.; Ubachs, W.; Salumbides, E. J. CARS spectroscopy of the ($v = 0 \rightarrow 1$) band in T_2. *J. Phys. B* **2017**, *50*, 214004.

(46) Trivikram, T. M.; Schlösser, M.; Ubachs, W.; Salumbides, E. J. Relativistic and QED Effects in the Fundamental Vibration of T_2. *Phys. Rev. Lett.* **2018**, *120*, 163002.

(47) Lai, K.-F.; Czachorowski, P.; Schlösser, M.; Puchalski, M.; Komasa, J.; Pachucki, K.; Ubachs, W.; Salumbides, E. J. Precision tests of nonadiabatic perturbation theory with measurements on the DT molecule. *Phys. Rev. Research* **2019**, *1*, 033124.

(48) Cozijn, F. M. J.; Diouf, M. L.; Ubachs, W.; Hermann, V.; Schlösser, M. Precision Measurement of Vibrational Quanta in Tritium Hydride. *Phys. Rev. Lett.* **2024**, *132*, 113002.

(49) Lai, K.-F.; Hermann, V.; Trivikram, M.; Diouf, M.; Schlösser, M.; Ubachs, W.; Salumbides, E. Precision measurement of the fundamental vibrational frequencies of tritium-bearing hydrogen molecules: T_2, DT, HT. *Phys. Chem. Chem. Phys.* **2020**, *22*, 8973–8987.

(50) Tiesinga, E.; Mohr, P. J.; Newell, D. B.; Taylor, B. N. CODATA recommended values of the fundamental physical constants: 2018. *Rev. Mod. Phys.* **2021**, *93*, 025010.

(51) Yerokhin, V. A.; Pachucki, K.; Patkóš, V. Theory of the Lamb Shift in Hydrogen and Light Hydrogen-Like Ions. *Annalen der Physik* **2019**, *531*, 1800324.

(52) Korobov, V. I.; Hilico, L.; Karr, J.-P. Fundamental Transitions and Ionization Energies of the Hydrogen Molecular Ions with Few ppt Uncertainty. *Phys. Rev. Lett.* **2017**, *118*, 233001.

(53) Liu, J.; Salumbides, E. J.; Hollenstein, U.; Koelemeij, J. C. J.; Eikema, K. S. E.; Ubachs, W.; Merkt, F. Determination of the ionization and dissociation energies of the hydrogen molecule. *J. Chem. Phys.* **2009**, *130*, 174306.

(54) Hölsch, N.; Doran, I.; Merkt, F.; Hussels, J.; Cheng, C.-F.; Salumbides, E. J.; Bethlem, H. L.; Eikema, K. S. E.; Beyer, M.; Ubachs, W.; Jungen, C. Ionization and dissociation energies of HD and dipole-induced g/u-symmetry breaking. *Phys. Rev. A* **2023**, *108*, 022811.

TOC Graphic